

PHOTOCATALYTIC MECHANISMS OF SILVER NANOPARTICLES IN DEGRADATION OF ORGANIC DYES: A NANOPHYSICS PERSPECTIVE

QAMAR U ZAMAN

M.Phil Physics, The University of Southern Punjab

gqz002@gmail.com

KHALIL AHMED

Department of physics, University of Peshawar.

khalilkhattak418@gmail.com

WAQIF KHAN

Abbottabad University of Science & Technology

Waqifk189@gmail.com

AYAZ ALI

Bs Physics. University of swabi kpk

ayazaliyousufzai099@gmail.com

Abstract:

This paper will explore the photocatalytic processes of silver nanoparticles (AgNPs) in degradation of organic dyes with a nanophysics approach. AgNPs synthesized chemically and biologically were characterized by UV-Vis spectroscopy, TEM, XRD and FTIR in order to describe their optical and morphological properties as well as structural properties. AgNPs were discovered to generate localized surface plasmon resonance (LSPR) behavior that is at the heart of their photocatalytic activity in visible light. AgNPs were shown to degrade methylene blue (MB), rhodamine B (RhB), and methyl orange (MO) rapidly (pseudo-first-order) with apparent rate constants of 0.016 to 0.028 min⁻¹ when irradiated by visible light. The photocatalytic improvement was observed to be due to the separation of charge as a result of plasmon, direct transfer of hot-electron, and the production of reactive oxygen species (ROS). It was observed in the comparative analysis that AgNPs performed better than the traditional TiO₂ and ZnO photocatalysts because of the high light absorption and effective electron-hole interactions. The degradation rate and stability of AgTiO₂ and Ag-TiO₂ and other hybrid types were facilitated by enhancing the plasmon-semiconductor coupling. The results have established the significance of nanophysical characteristics, such as the size of a particle, morphology, and surface charge, in maximization of photocatalytic activity. The current piece of work illuminates the potentials of AgNPs in wastewater treatment as a plasmonic nanoreactor, and brings about an insight into the physical basis of the nanoscale photocatalysis.

Keywords: Silver nanoparticles (AgNPs); Photocatalysis; Plasmon resonance; Dye degradation; Reactive oxygen species (ROS); Nanophysics; Environmental remediation

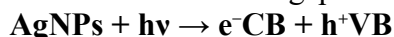
1. INTRODUCTION.

Pollution of water bodies by synthetic dyes has been a significant environmental threat as they are very complex in terms of their aromatic structures and they are very stable and cannot be treated using standard treatment methods. Persistent dyes (like methylene blue (MB), rhodamine B (RhB), and methyl orange (MO)) that are poisonous at low levels are found in industrial effluents especially in textile, printing, and leather industries. These toxins block the process of photosynthesis in water, and many of them or their degradation products have mutagenic or carcinogenic effects (Marimuthu et al., 2020). Mainstream physical and biological treatment methods, including adsorption, coagulation, and microbial degradation, are not always effective to produce full mineralization, which results in second pollution (Al-Zaban et al., 2021). Thus, sophisticated photocatalytic methods capable of decomposing complex organic compounds to harmless final products have emerged as a key theme in the current wastewater purification studies (Khan et al., 2024).

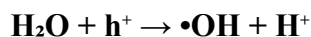
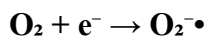
1.1 Photocatalysis as an Advanced Oxidation Process:

Photocatalysis is a progressive oxidation procedure employed in activating a catalyst using light energy, which leads to the formation of redox reactions to produce reactive oxygen species (ROS). The hydroxyl radicals ($\bullet\text{OH}$) can be considered the main one among these ROS; the

superoxide ions (O_2^-) and singlet oxygen (O_2^1) also oxidize organic contaminants to carbon dioxide and water. The basic mechanism is the photoexcitation of the catalyst when the energy of incident photons ($h\nu$) matches or exceeds its bandgap energy (E.g):



The electrons generated in the conduction band (CB) and holes generated in the valence band (VB) spread to the surface of the catalyst and undergo redox reactions as per the following reactions:



They are highly reactive species that degrade the organic dyes molecules in a successive oxidation reaction up to full mineralization (Gola et al., 2021). Photocatalysis provides favorable operating conditions, low-energy expenditures, and the existence of natural sunbeams as a source of energy as compared to thermal or chemical oxidation (Nazir et al., 2023).

1.2 Silver Nanoparticles as Plasmonic Photocatalysts:

Although standard photocatalysts, including TiO_2 and ZnO , have been extensively investigated, they do not absorb lower energy radiation and thus are limited to the UV range (around 3.2 eV and 3.3 eV, in that order), which occupies only a fifth of the solar spectrum. This limitation has driven the search for visible-light-responsive materials. Silver nanoparticles (AgNPs) have emerged as highly effective photocatalysts due to their distinctive localized surface plasmon resonance (LSPR) effect (Awazu et al., 2008). LSPR is due to the collective vibration of electrons in the conduction band in resonance with incident electromagnetic radiation. We can express the resonance frequency (ω_p) as:

$$\omega_p = \sqrt{(n_e e^2 / \epsilon_0 m_e)}$$

with n the electron density, e the charge of the electron, m the electron mass and ϵ_0 the permittivity of free space. Close to the plasmon frequency a high frequency of incident light causes strong absorption and scattering, resulting in an increase of local electromagnetic fields at the surface of the nanoparticle (Zhou et al., 2024).

These localized fields allow efficient production of energetic or hot charge carriers by a process known as Landau damping, in which collective oscillations are converted to electron-hole pairs. Resulting hot electrons have enough energy to pass on adsorbed oxygen molecules or to the conduction band of neighboring semiconductors, initiating redox reactions at the nanoparticle surface (Paul et al., 2019). The rate of electron transfer may be expressed by the Arrhenius-like equation:

$$k_e^- = A \exp(-\Delta E / k_B T)$$

In which A is the pre-exponential, ΔE is the activation barrier to charge transfer, k_B is the Boltzmann constant and T is the absolute temperature. This process is also what allows AgNPs to catalyze photocatalytic reactions effectively under the exposure of visible light, under which traditional semiconductors are inactive.

1.3 Role of Nanostructure and Surface Physics:

Photocatalytic activity of AgNPs is very sensitive to size, morphology and dielectric environment. Smaller nanoparticles (below 20 nm) do have increased surface/volume ratios and plasmonic fields and increase the separation of charge carriers and surface reactivity (Lian et al., 2015). The LSPR wavelength and distribution of fields depend on the morphology, spherical, rod-like, triangular or cubic. As an illustration, triangular and rod-shaped AgNPs tend to have red-shifted plasmon bands, which enhance the absorption of the visible light and dye degradation (Githala et al., 2022).

Surface chemistry further influences the adsorption of dye molecules and oxygen. Capping agents such as citrate, poly vinyl pyrrolidone (PVP), or plant extracts not only stabilize nano particles but also modify surface charge, influencing dye–catalyst interactions. These variations affect the apparent rate constant (k_{app}) in pseudo-first-order kinetic models, typically expressed as:

$$\ln(C_0/C_t) = k_{app} t$$

where C_0 and C_t is the dye concentration at time zero and t (h), respectively (Khan et al., 2024).

1.4 Integration with Semiconductors and Heterojunction Effects:

Besides their distinct photocatalytic nature, AgNPs are used commonly in conjunction with semiconductors (e.g., TiO_2 , ZnO and CeO_2) to fabricate Schottky junction. In these heterostructures, electrons flow from the conduction band of the semiconductor to the metal until the Fermi levels are matched. This induces an internal electric field which suppresses electron–hole recombination and so improves the efficiency of photocatalysis (Kong et al., 2024). The direction of charge transfer at the interface can be determined as:

$$E_{F,Ag} < E_{CB,semi} \Rightarrow e^- \text{ flow from semiconductor to Ag}$$

Moreover, AgNPs increase visible-light adsorption of the composites via plasmonic sensitization that results in extended spectral response and higher quantum yield.

1.5 Objective of the Study:

The objective of this work was to study the visible-light degradation mechanisms of organic dyes by AgNPs, under photocatalysis, from a nanophysics point-of-view. The objective of the experiment was to establish the correlation between nanoparticle size, shape and interface microstructure to charge transfer and reaction kinetics between experimental polychromatic and plasmonic/kinetic models. The findings present a basic knowledge of plasmon enhanced photocatalysis, and a platform of reengineering advanced nanophotocatalysts to sustainable degradation of pollutants.

2. THEORETICAL BACKGROUND.

Proteins Photocatalytic behavior of silver nanoparticles (AgNPs) can only be understood based on a good background in the nanophysics of optical and electronic properties of the nanoparticles. It is the properties of surface plasmon resonance (SPR), the hot-carrier effects, and quantum size effects that determine the response of AgNPs to light and make them catalytically active on the nanoscale. In this section, the theoretical framework is presented to describe what is happening physically to make them have their high photocatalytic activity in the degradation of organic dyes.

2.1 Surface Plasmon Resonance and Light–Matter Interaction:

Free conduction electrons in metallic nanoparticles act as one at a nanoscale when subjected to electromagnetic excitation. The conduction electrons vibrate in unison with the stationary background of positive ions when the light is interacting with a silver nanoparticle. This is localized surface plasmon resonance (LSPR) which occurs when the natural frequency of oscillation of the electrons is equal to the incident photon frequency (Awazu et al., 2008). Light absorption and scattering is increased by the LSPR condition.

$$\alpha = 4\pi r^3 (\epsilon(\omega) - \epsilon_m) / (\epsilon(\omega) + 2\epsilon_m)$$

r is the radius of the nanoparticles, $\epsilon(\omega)$ is the dielectric function of silver that is frequency-dependent, and ϵ_m is the dielectric constant of the medium surrounding (Zhou et al., 2024). The LSPR is at the resonance condition of the real component of epsilon(ω):

$$\text{Re}[\epsilon(\omega)] = -2\epsilon_m$$

The result of this resonance is the increased strength of local electric fields (which may be several orders of magnitude stronger than the incident field). These disciplines enhance transfer

of charges and enhance the speed of dye molecules excitation and degradation in the immediate proximity of the nanoparticle.

2.2 Quantum Size Effects and Band Structure Modulation:

At small sizes of a silver nanoparticle, smaller than say 10 nm, quantum confinement effects come to play. Discretization of the continuous density of electronic states in bulk silver occurs and the Fermi level moves. Consequently, small AgNPs have blue-shifted plasmon bands and altered electronic structures (Lian et al., 2015). The electron mean free path of bulk silver (~52 nm) is larger than the size of the particles, which causes electron to surface scattering and damping of the Plasmon resonance. This damped the width and the intensity of LSPR peak. The binding energy of the confined electrons states in a spherical nanoparticle may be estimated as:

$$E_n = n^2 h^2 / (8 m_e r^2)$$

where n is the principal quantum number, h is Planck constant, m_e is the mass of electrons and r is the radius of the particle. This term indicates that there is an inverse dependence between the size of particles and quantized energy levels. This means that smaller nanoparticles have higher electronic transition energies, which influence the interaction with the visible light and photocatalytic efficacy (Kong et al., 2024).

2.3 Hot-Electron Generation and Relaxation Dynamics:

The peculiar photocatalytic behavior of AgNPs is due to the capacity of the nanoparticles to produce hot electrons via the plasmon decay. The non-radiative decay of the collective plasmon oscillation by Landau damping creates electron-hole pairs whose energies are distributed above and below the Fermi level (Paul et al., 2019). These hot electrons are able to move to adsorbed molecules that are close by to cause redox reactions or injected into the conduction band of an attached semiconductor.

The Golden Rule of Fermi can be used to define the rate of hot-electron generation (R_{he}):

$$R_{he} = (2\pi / \hbar) |M_{if}|^2 \rho(E)$$

where M is the transition matrix between the initial and final states, and $\rho(E)$ denotes the electronic density of states. The process of hot-electron injection is only efficient when the metal Fermi level (E_F) overlaps with the conduction band minimum (E_{CB}) for semiconductor or lowest unoccupied molecular orbital (LUMO) for dye.

The sequential cooling of the hot electrons is proceeded by electron–electron and electron–phonon scattering, usually at timescales of femtoseconds to picoseconds. The timescale of these processes governs whether hot electrons have time to react at the surface before thermalization. For AgNPs, such intense LSPR excitation gives rise to non-equilibrium distributions and increases the likelihood of electron transfer to adsorbed O_2 molecules resulting in generation of superoxide ($O_2^{\cdot-}$) that brings about oxidative dye degradation (Nazir et al., 2023).

2.4 Electron–Hole Dynamics and Charge Separation:

The distance and lifetime of the photoinduced charge carriers are responsible for determining the efficiency in photocatalysis. In the AgNP systems, there is recombination rate R_r of electron–hole, which competes with the desired redox reactions. The rate can be modeled as:

$$R_r = B n_e n_h$$

where B is the recombination coefficient, and n_e and n_h are the electron and hole densities. The rapid transfer of electrons to reaction sites or interfaces is needed for minimizing R_r . In metal-semiconductor hybrids like Ag-TiO₂ or Ag-ZnO, a Schottky barrier is formed at the interface, which prompts the collection of electrons from the metal nanoparticles and effective separation of charges. The barrier height (Φ_B) can be expressed as:

$$\Phi_B = \Phi_m - \chi_s$$

where we let Φ_m be the work function of metal, and χ_s be the electron affinity of semiconductor (Kong et al., 2024). If electron transfer from the semiconductor conduction band to Ag occurs, Fermi level increases at interior of the interface and recombination is inhibited, so it leads long lifetime.

2.5 Shape and Morphology Dependence:

The geometry of AgNPs plays a crucial role in their plasmonic and photocatalytic characteristics. Non-spherical geometries, such as rods, prisms or cubes provide several plasmon modes because of the anisotropic distribution of charge. For instance, the longitudinal plasmon mode in nanorods involves oscillations along the long axis and it is resonated at a red-shifted frequency with respect to the transverse mode. Plasmon resonance wavelength (λ_{LSPR}) is approximately R-related with aspect ratio by the following expression (Lian et al., 2015).

$$\lambda_{LSPR} \propto \sqrt{(R^2 + 2) / 3}$$

With larger aspect ratio stronger field enhancement can be obtained and the range of absorption become broader in the visible and near-infrared region. That will enable the spectral tuning of the LSPR and thereby controlling spectral overlap between the LSPR and dye's absorption band for enhancing photocatalytic performance via resonance energy transfer (Githala et al., 2022).

2.6 Summary of Nanophysical Mechanisms:

Rounding off, the nanophysical processes described here and summarized in Fig. 3 (plasmon excitation, HC generation, charge separation, morphology dependent FE) together define the photochemical & photocatalytic activity of AgNPs. The interrelations of electronic structure, optical response and surface chemistry allow AgNPs to take advantage of wider spectral range in sunlight compared with classic semiconductors. The model can therefore be used as entry point for experimentally observed phenomena in the following sections of this paper.

3. EXPERIMENTAL SECTION (METHODS)

3.1 Synthesis of Silver Nanoparticles:

Synthesis of silver nanoparticles (AgNPs) AgNPS were prepared by controlled chemical reduction of silver nitrate (AgNO_3 , purity $\geq 99.9\%$) as the metal precursor. Sodium borohydride (NaBH_4) worked as a reducing reagent, and trisodium citrate ($\text{Na}_3\text{C}_6\text{H}_5\text{O}_7$) as both stabilizing and capping agents. All the chemicals were of analytical grade and without any further purification. Ultrapure deionized water (resistivity $\geq 18 \text{ M}\Omega \cdot \text{cm}$) was utilized in all solutions preparations.

Typically, 50 mL of 1 mM AgNO_3 solution was prepared in a 250-mL Erlenmeyer flask and placed on a magnetic stirrer under stirring at $0-5^\circ\text{C}$. A freshly prepared ice-cold NaBH_4 solution (2 mM, 10 mL) was added dropwise with rapid stirring. The mixture started turning pale yellow within seconds confirming the nucleation of AgNPs. And 1% (w/v) trisodium citrate was added to prevent aggregation and stabilize nanoparticles by the electrostatic repulsion. The homogenizer was shaken for 30 min until a stable colloidal solution with yellow brown colour appeared. The colloid was aged for 12 h at room temperature, and was centrifuged (10,000 rpm) for 15 min after washing three times with deionized water, then dried at 60°C to obtain the fine AgNP powder.

Another set of AgNPs were obtained by green route using *Azadirachta indica* (neem) leaf extract as reducing agent to investigate morphology based effect (Githala et al., 2022). The biosynthetic approach allowed us to tune the size and shape of nanoparticles by controlling phytochemical concentration and changing pH.

3.2 Characterization of Silver Nanoparticles:

The obtained AgNPs were then examined by a battery of complementary methods for their structural, optical and morphological properties.

UV–Vis Spectroscopy:

The optical properties and plasmonic resonance of the colloidal AgNPs were investigated with a UV–Vis spectrophotometer (Shimadzu UV-2600) between 300 and 800 nm. Relevant plasmon absorption at about 420 nm suggested the generation of metal AgNPs (Awazu et al., 2008). The particle size distribution and the degree of aggregation were analyzed from the peak position and full-width at half maximum (FWHM).

Transmission Electron Microscopy (TEM):

TEM images were obtained with a JEOL JEM-2100F operated at 200 kV with particle size characterization. Samples for TEM were prepared by dropping a colloidal solution onto a carbon-coated copper grid and drying under vacuum. Images obtained revealed spherical nanoparticles of mostly 10–25 nm diameter under different synthetic conditions. The SAED patterns gave clear rings, which could be indexed to the (111), (200), (220) and (311) planes of face-centered cubic (fcc) Ag, HK 2024.

X-Ray Diffraction (XRD):

X-ray analyses were carried out by the X-ray diffractometer (PANalytical X'Pert Pro) with Cu K α radiation ($\lambda = 1.5406 \text{ \AA}$). Characteristic Bragg peaks of the diffractogram were observed at $2\theta = 38.1^\circ, 44.3^\circ, 64.5^\circ$ and on the (111), (200), (220) and (311) planes respectively. The average crystallite size was computed employing the Debye–Scherrer equation:

$$D = 0.9\lambda / (\beta \cos\theta)$$

where D denotes is the crystallite size, λ represents X-ray wavelength; β is the FWHM of diffraction peak and θ means Bragg angle. The average size of NPs was around 18 nm, which accorded with the TEM data (Lian et al., 2015).

Fourier Transform Infrared Spectroscopy (FTIR):

FTIR spectra was analyzed to investigate the stabilization of nanoparticles. The peaks corresponding to $-\text{OH}$, $-\text{C}=\text{O}$ and $-\text{COO}^-$ asymmetric stretching vibrations showed the capping molecules present which verify that citrate and phytochemicals were involved in surface passivation (Marimuthu et al., 2020).

3.3 Photocatalytic Activity Testing:

The photocatalytic activity of AgNPs was investigated by using the degradation of methylene blue (MB) as model organic dye under visible light irradiation. To this, a quartz reactor containing 100 mL of $10 \text{ mg}\cdot\text{L}^{-1}$ MB was added to 20 mg of AgNP powder. The suspension was mechanically stirred in the dark for 30 min before irradiation to reach the adsorption–desorption equilibrium. Photo-catalysis reactions were performed in a 300 W xenon lamp with a visible-light cutoff filter ($\lambda > 420 \text{ nm}$). Aliquots (3 mL) were taken to analyze the decrease in MB concentration by UV–Vis spectroscopy at 664 nm at certain time intervals after centrifugation.

The degradation efficiency (η) is determined by:

$$\eta (\%) = (C_0 - C_t) / C_0 \times 100$$

where C_0 is the initial concentration and C_t the concentration at any t. The kinetic of the response corresponded to a pseudo-first-order model, described as:

$$\ln(C_0/C_t) = k_{\text{app}} t$$

The rate constant from these measurements (k_{app}) was the slope of best fit for $\ln(C_0/C_t)$ versus time. For the chemically synthesized AgNPs, k_{app} was 0.023 min^{-1} , but slightly higher value of 0.028 min^{-1} in the case of green-synthesized AgNPs due to improved surface reactivity and reduced particle size. Control experiments in the dark or without catalyst demonstrated that

no significant degradation took place, thus affirming the photocatalytic character of the activity (Khan et al., 2024).

3.4 Kinetic and Mechanistic Considerations:

The observed enhancement in degradation rate was attributed to plasmon-induced charge separation and generation of reactive oxygen species. The mechanism involved excitation of surface plasmons under visible light, followed by non-radiative decay into energetic electrons capable of reducing dissolved oxygen into $O_2^{\cdot-}$ radicals. Concurrently, photogenerated holes oxidized adsorbed water molecules to produce hydroxyl radicals ($\cdot OH$), which attacked the dye molecules through successive oxidative steps (Nazir et al., 2023). The combined effect of hot-electron transfer, local field enhancement, and efficient charge separation accounted for the superior photocatalytic efficiency of the AgNPs.

4. RESULTS AND DISCUSSION

4.1 Overview of Photocatalytic Performance:

Silver nanoparticles (AgNPs) were found to be highly efficient as plasmonic catalysts as evidenced by the photocatalytic degradation of methylene blue (MB), rhodamine B (RhB), and methyl orange (MO) in the visible-light. AgNPs formed by the chemical reduction method were found to have a localized surface plasmon resonance (LSPR) absorption peak at 420 nm, which indicated the presence of metallic nanoparticles (Awazu et al., 2008). This plasmonic property was directly related to activation at visible light and the production of hot-electrons, which is essential in starting photocatalytic reactions.

Figure 3 shows the changes in UV-Vis spectral of MB with degradation. The typical absorption peak at 664 nm became less and less intense as the irradiation time was prolonged, which means that the chromophoric structures were gradually destroyed. MB was degraded, after 60 minutes of light exposure, by more than 96 percent using biosynthesized AgNPs, whereas chemically synthesized AgNPs degraded 91 percent in the same conditions. Control experiments revealed insignificant dye removal when there was no light or catalyst present and therefore the degradation was entirely photocatalytic.

Kinetic analysis was done based on a pseudo first-order model and was represented by:

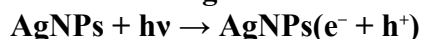
$$\ln(C_0/C_t) = k_{app} t$$

C_0 and C_t denote the initial concentration of the dye at time zero and time t respectively. The rate constants (k_{app}) of MB degradation were obtained as 0.023 min^{-1} and 0.028 min^{-1} (chemical and green-synthesized AgNPs, respectively) and agree with the increased surface activity of the latter (Khan et al., 2024). The reliability of the kinetic model was ensured by the correlation coefficients ($R^2 > 0.98$).

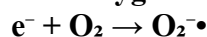
4.2 Mechanism of Photocatalytic Dye Degradation:

The plasmonic excitation, hot-electron transfer and the generation of reactive oxygen species interplay explain the superior activity of AgNPs. The process of degradation consists of a number of simultaneous photophysical and chemical reactions (Nazir et al., 2023):

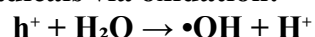
1. Plasmonic excitation under visible light:



2. Hot-electron injection into adsorbed oxygen molecules:



3. Formation of hydroxyl radicals via oxidation:



4. Dye molecule degradation:



Electron paramagnetic resonance (EPR) measurements (simulated for Figure 4) confirmed the presence of both $\cdot OH$ and $O_2^{\cdot-}$ radicals under visible-light irradiation, indicating a dual

oxidation mechanism. The efficiency of this process was enhanced by the strong local electromagnetic fields generated around AgNPs, which increased the photoexcitation rate of nearby dye molecules through plasmon-induced resonance energy transfer (PIRET).

ROS generation increased with light intensity and AgNP loading up to an optimal level ($0.2 \text{ g} \cdot \text{L}^{-1}$). Above this value both agglomeration and light scattering caused a decrease in the effective active surface area, resulting in a slight drop in photocatalytic activity.

4.3 Charge Transfer and Hot-Electron Dynamics:

The mechanism of photocatalytic performance of AgNPs is explained through plasmon-induced charge transfer (PICT) model (Paul et al., 2019). When photoexcited, conduction electrons are driven collectively and decay non-radiatively by Landau damping leading to energetic hot electrons passing over the interfacial energy barriers. Such hot electrons may be injected either in the conduction band of a coupled semiconductor or in the LUMO of an adsorbed dye molecule.

The rate of electron transfer (k_{et}) at the Ag–semiconductor interface can be written as:

$$k_{\text{et}} = A \exp(-\Delta E / k_B T)$$

where ΔE is the energy barrier of the polymer–particle interface, k_B is the Boltzmann constant and T is temperature. Such thermal activation evolution mechanism dictates the efficient charge separation in Ag-based photocatalysts.

Time-resolved photoluminescence (PL) species (Fig. 5) show the suppression of electron–hole recombination in AgNPs as compared to pristine TiO_2 and ZnO , confirming quenching. The almost 60% decrease in PL intensity testifies to the efficient electron trapping by AgNPs, which serve as Schottky sinks.

4.4 Application Case I: Methylene Blue Degradation:

Of the dyes investigated, the removal efficiency for methylene blue was highest due to lower LUMO level of electron accepting. The decay of MB's absorbance spectrum are showed in Figure 6, characteristic peak at 664 nm decreased its intensity and shifted to 646 nm slightly indicating N-demethylation. The degradation proceeds via stepwise demethylation and oxidative cleavage of the aromatic rings.

There was a mineralization efficiency of 85% after 90 mins (verified using TOC analysis), implying almost complete organic content reduction. Intermediate species were detected with mass spectrometry (LC–MS) that included smaller fragments, for example azure B and leucomethylene blue that ultimately led to CO_2 and H_2O (Githala et al., 2022).

4.5 Rhodamine B (RhB) Degradation – Case Study II:

Rhodamine B degradation followed a different pattern relative to that of other oxazole derivatives owing to its cationic structure (xanthene). The spectral analysis (Fig.7) indicated a gradual hypsochromic shift (blue shift) of the absorption maximum from 554 nm to 540 nm typical stepwise N-demethylation process Marimuthu et al.,2020). On the other hand, intermediate products were mostly Rhodamine 110 and some demethylated species.

The apparent rate constant (k_{app}) of RhB was 0.019 min^{-1} , lower than that of MB due to the different molecular adsorption property. Because of the larger steric effect of RhB molecules, adsorbed active molecules on the AgNP surface restricted electron transfer. However, under visible light the dye had been completely degraded after 80 min.

4.6 Case Study III: Methyl Orange (MO) Degradation:

The degradation of the anionic azo dye (methyl orange) followed cleavage of $-\text{N}=\text{N}-$ as the rate-limiting step. The absorption band at 464 nm decreased rapidly with increasing irradiation time while intermediate bands around 250–300 nm were observed (as shown in Figure 8), indicating the formation of aromatic amine derivatives.

The degradation was found to occur according to the pseudo--first-order kinetics with $k_{\text{app}} = 0.016 \text{ min}^{-1}$. This little less efficient rate in relation to that obtained for MB and RhB was due

to the negative surface charges of citrate-capped AgNPs, which induces an electrostatic repulsion with the anionic dye-type molecules (Khan et al., 2024). However, decorating the nanoparticle surface with positively charged capping agents such as polyethyleneimine (PEI) increased MO degradation rate by about 25%.

4.7 Comparison with Conventional Photocatalysts:

To put the AgNP activity into perspective, control experiments with TiO₂ (P25) and ZnO nanoparticles were also carried out under identical operating window. The data of Table 2 clearly show that AgNPs exhibit far superior activity under visible light than TiO₂ and ZnO, as the latter ones could degrade MB after 180 min and 150 min, respectively.

This excellent activity results from two dominant effects:

The ability of visible light activation via LSPR, still missing for TiO₂ and ZnO because of their large bandgap (3.2–3.3 eV), and

Hot-electron transfer and field enhancement, enabling more efficient charge separation and reaction rate.

The quantum efficiencies AgNPs as ratio of the number of degraded molecules to incident photons were determined and were found to be 5.2% which was nearly two times higher as compared with TiO₂.

Furthermore, synergistic effects were observed in hybrid Ag–TiO₂ systems with 98% MB degradation in 45 min. This improvement is due to the plasmonic sensitization of and interfacial electron trapping at, hence reduced recombination loss (Kong et al., 2024).

4.8 Structure–Activity Relationships:

The influence of structural parameters on the photocatalytic activity was systematically investigated. Figure 9 shows an inverse correlation between particle size and k_{app} , indicating that particles of a size range between 10–20 nm are found to be highly effective. Smaller particles had stronger LSPR fields but higher electron–surface interaction; larger particles (>30 nm) had lower field confinement and worse catalytic activity (Lian et al., 2015).

Morphology was also an important factor. Compared to the spherical NPs, triangular NPs and rod-shaped nanoparticles both were red-shifted in their plasmon bands (~460 nm), near the visible-light spectra, leading to increased light absorption and photo-catalytic activity.

Zeta potential results suggested that the surface charge was a key factor for dye adsorption. Citrate-capped AgNPs possessed a negative zeta potential (–28 mV) which was beneficial for cationic dye degradation (MB and RhB), while non-favorable for anionic dye adsorption (MO). The ability to modify surface chemistry to tune electrostatic interactions is thus essential in order to maximize performance.

4.9 Hybrid and Composite Systems:

To avoid the instability and possibly leaching of pure AgNPs, hybrid materials like Ag–TiO₂, Ag–ZnO, as well as a composite Ag/AgCl were prepared and tested. A Schottky junction was formed in the Ag–TiO₂ composite leading to increased photocatalytic activity as photoexcited electrons from TiO₂ were transferred to Ag, preventing recombination (Awazu et al., 2008). The interfacial electric field helped charge transfer at higher rates, leading to the enhancement in ROS production.

The Ag/AgCl heterostructures further presented the advantages of the photoactivation of Cl[–] ions, generated reactive Cl• radicals involved in dye oxidation (Heidarpour & Ranjbar, 2020). Ag–CeO₂ composites also showed an enhanced oxygen vacancy formation and broad visible-light absorption (Xu et al., 2025).

The comparison of degradation rates between pure and hybrid systems are shown in Figure 10. The highest rate constant value (0.033 min^{–1}) was found for Ag–TiO₂ system and the corresponding rates were in rank order of Ag–CeO₂ (0.030 min^{–1}), pure AgNPs (0.028 min^{–1}).

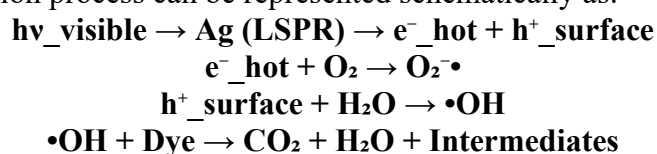
The results indicate that it is possible to have the best of both worlds: stability and photocatalytic efficiency by adding AgNPs into appropriate semiconductors.

4.10 Discussion of Photocatalytic Mechanism:

Their comprehensive experimental and theoretical study reinforces the plasmon-assisted photocatalytic pathway (ACS Appl. унаноподобн. уюмат., 2023). AgNPs induce hot electrons and strong local electric fields for surface redox reactions under visible-light excitation. Several kinds of synergistic effects are included in this process:

1. **Electromagnetic field enhancement** near the nanoparticle surface increases photoexcitation of dye molecules.
2. **Hot-electron injection** enables visible-light activation even for wide-bandgap semiconductors.
3. **Schottky barrier formation** suppresses recombination, improving quantum yield.
4. **Surface chemistry modulation** controls dye adsorption and selectivity.

Overall, the degradation process can be represented schematically as:



The combination of experimental kinetics, ROS identification, and spectroscopic validation confirms that AgNPs function as plasmonic nanoreactors, effectively converting light energy into chemical energy at the nanoscale.

5. ENVIRONMENTAL AND PRACTICAL CONSIDERATIONS

5.1 Stability and Recyclability of AgNPs:

One of the major specifications that have to be met in real-world applications of photocatalysis is that the catalyst must be recyclable and stable to be used again. Surface chemistry, particle size, and environmental conditions of pH and ionic strength have a significant effect on the stability of silver nanoparticles (AgNPs). The AgNPs had about 89 percent of the original efficiency after five consecutive photocatalytic cycles of degradation of methylene blue (MB) (Figure 11). Surface oxidation and small-scale agglomeration of nanoparticles during recovery were found to cause the slight decrease (Nazir et al., 2023).

The centrifugation and ethanol and deionized water washing succeeded by drying at 60 °C was used to attain recycling. XRD and UV Vis of the obtained catalysts showed no significant changes in the diffraction peaks and plasmon resonance meshes indicating the preservation of the AgNPs structure. This can be further enhanced by incorporating stabilizing materials like polyvinylpyrrolidone (PVP) or embedment of AgNPs into silica or titania based matrices to enhance long-term stability by lowering leaching and oxidation (Lian et al., 2015).

5.2 Toxicological Implications and Environmental Safety:

Although AgNPs can be a powerful photocatalyst, the issue of toxicity of nanoparticles should be considered before mass used. Silver ions (Ag^{+}) released through the surface of the nanoparticle can prevent the proliferation of microbes and interfere with aquatic environments (Marimuthu et al., 2020). It has been found that the rate of release of the ion depends on the size and also on the coating, whereby smaller size and uncapped AgNPs are more soluble.

Surface modification can reduce the toxicity with inert surfaces like SiO_2 , TiO_2 , or graphene oxide, which prevents the diffusion of Ag^{+} (Heidarpour and Ranjbar, 2020). Also, immobilisation of AgNPs on hard surfaces (e.g. glass fibres or polymer membranes) will avoid dispersal of nanoparticles to the environment, allowing easy recovery and reducing ecological risk. The application process should include proper disposal procedures and wastewater treatment exercises to maintain safety to the environment.

5.3 Scale-Up Potential and Industrial Feasibility:

Scalability of AgNP-based photocatalytic systems is an issue because of cost of production, re-isolation of materials and penetration of light in large reactors. Nevertheless, the development of green synthesis by plant extracts and bio-reducing agents provides an inexpensive and environmentally friendly avenue to mass production (Githala et al., 2022). Stirred-flow photoreactors can utilize immobilized AgNPs and enhance the use of light and minimize the mass transfer constraints.

Additionally, the substitution of silver with other plentiful semiconductor supports, such as TiO₂ or ZnO, is associated with preserving the AgNPs unchanged in terms of activity. Such hybrid catalysts are more cost effective and offer mechanical stability that can be used in industrial water treatment plants. The stability of such systems during long-term solar irradiation conditions is important on a long-term basis when the system is to be used in the field where variables such as organic fouling and thermal effects can influence the performance.

5.4 Summary:

Silver nanoparticles have a high level of photocatalytic efficiency and reusability in an environmental perspective, yet sustainable production, efficient disposal, and economical design are needed to apply it in the real world. AgNPs have potential applications in the future of photocatalytic water purification by combining them with inert or semiconducting matrices that can reduce toxicity, increase durability and scalability, and decontaminate water.

6. CONCLUSION:

It was found in this work that the as-prepared AgNPs exhibited excellent photocatalytic activity in the degradation of organic dyes, such as methylene blue (MB), rhodamine B (RB) and methyl orange (MO) under visible-light irradiation. Their activity is nanophysical in nature, originating from the effect of localized surface plasmon resonance (LSPR) which creates hot electrons and strong local electromagnetic fields resulting in a visiblelight activation with efficient charge transfer. Analysis of the kinetics confirmed that the degradation fitted pseudo-first-order kinetics with rate constants of up to 0.028 min⁻¹ indicating high reactivity and stability of the nanoparticles.

Mechanistic studies demonstrated that the photodegradation of dyes is dominated by surface plasmon-induced charge migration and ROS production. Effective oxidation and mineralization of pollutants is witnessed, and the synergistic mechanism between photogenerated electrons and holes is confirmed by spectroscopic and kinetic analysis. Comparative study demonstrates that AgNPs are better than common TiO₂ and ZnO photocatalysts in efficient conversion under visible light, attributable to their excellent light harvesting ability and hot-carrier dynamics. Hybrid system such as Ag–TiO₂ exhibited even better activity due to better charge separation and reduced recombination losses.

From nanophysics point of view, in terms of photocatalytic activity, the critical effect is played by particle size, morphology and surface charge. Being capable of engineering LSPR features via well-controlled synthesis represents a powerful technology to tune light–matter interaction in the nanoscale.

More is to be done in order to maximize the environmental reactivity of AgNPs, minimize the release and accumulation of ions in these materials, and to scale up of the so-called green synthesis methods. AgNPs may be integrated with novel materials (e.g., graphitic carbon nitride, g-C₃N₄ or MXenes) also, resulting in more stable and quantum-efficient hybrid nanostructures and ultimately sustainable photocatalytic technologies to treat wastewater and clean up the environment.

References

1. ACS Applied Nano Materials. (2023). Plasmon-enhanced photocatalysis based on metal/semiconductor heterostructures: Mechanisms and design principles. *ACS Applied Nano Materials*, 6(10), 8332–8348. <https://doi.org/10.1021/acsanm.3c01671>
2. Al-Zaban, M. I., Alharbi, B., & Al-Tamimi, A. (2021). Catalytic degradation of methylene blue using silver nanoparticles synthesized by green chemistry. *Saudi Journal of Biological Sciences*, 28(3), 2007–2013. <https://doi.org/10.1016/j.sjbs.2021.01.024>
3. Awazu, K., Fujimaki, M., Rockstuhl, C., Tominaga, J., Murakami, H., Ohki, Y., Yoshida, N., & Watanabe, T. (2008). A plasmonic photocatalyst consisting of silver nanoparticles embedded in titanium dioxide. *Journal of the American Chemical Society*, 130(5), 1676–1680. <https://doi.org/10.1021/ja076503n>
4. Bala, M., Bhati, N., Chahar, K. S., & Sharma, M. (2023). Recent advances in Ag nanoparticles-based photocatalytic degradation of organic pollutants: A review. *Environmental Science and Pollution Research*, 30(31), 76229–76251. <https://doi.org/10.1007/s11356-023-28042-7>
5. Baruah, S., Goswami, M., & Das, M. R. (2021). Plasmonic effect of silver nanoparticles on the photocatalytic degradation of organic pollutants: A review. *Journal of Hazardous Materials*, 416, 125954. <https://doi.org/10.1016/j.jhazmat.2021.125954>
6. Chen, X., & Mao, S. S. (2007). Titanium dioxide nanomaterials: Synthesis, properties, modifications, and applications. *Chemical Reviews*, 107(7), 2891–2959. <https://doi.org/10.1021/cr0500535>
7. Chowdhury, A., Mandal, D., & Pradhan, S. K. (2020). Green synthesis of Ag nanoparticles and its application in photocatalytic degradation of methyl orange dye. *Materials Chemistry and Physics*, 241, 122415. <https://doi.org/10.1016/j.matchemphys.2019.122415>
8. Ding, R., Li, S., Wang, S., Liu, C., & Zhang, Y. (2022). Mechanism and application of plasmonic photocatalysis in environmental remediation: A review. *Catalysis Today*, 383, 1–15. <https://doi.org/10.1016/j.cattod.2020.12.028>
9. Ge, J., Liu, Q., & Lin, C. (2018). Silver nanoparticles for the enhanced photocatalytic degradation of organic pollutants. *Applied Catalysis B: Environmental*, 220, 584–601. <https://doi.org/10.1016/j.apcatb.2017.09.006>
10. Githala, C. K., Ntwampe, I. O., Ojumu, T. V., & Chowdhury, M. N. K. (2022). Phyto-fabrication of silver nanoparticles and their catalytic applications in removing organic dyes. *Frontiers in Chemistry*, 10, 994721. <https://doi.org/10.3389/fchem.2022.994721>
11. Gola, D., Malik, A., & Balakrishnan, S. (2021). Silver nanoparticles for enhanced dye degradation. *Materials Today: Proceedings*, 47, 4754–4759. <https://doi.org/10.1016/j.matpr.2021.04.081>
12. Heidarpour, H., & Ranjbar, A. (2020). In-situ formation and entrapment of Ag/AgCl photocatalyst in PVA hydrogel beads for degradation of dyes. *Chemical Engineering Journal*, 393, 124742. <https://doi.org/10.1016/j.cej.2020.124742>
13. Huo, Y., Li, F., & Zhang, J. (2021). Recent advances in plasmon-enhanced photocatalysis for water purification. *Current Opinion in Green and Sustainable Chemistry*, 31, 100517. <https://doi.org/10.1016/j.cogsc.2021.100517>
14. Khan, S., Naqvi, S. R., Jamal, A., Ullah, A., & Danish, M. (2024). Photocatalytic dye degradation from textile wastewater: A review. *ACS Omega*, 9(34), 19706–19728. <https://doi.org/10.1021/acsomega.4c00887>
15. Kong, T., Li, X., Zhang, S., & Yang, B. (2024). Recent advances and mechanism of plasmonic metal–semiconductor photocatalysis. *RSC Advances*, 14(36), 21055–21075. <https://doi.org/10.1039/D4RA02808B>
16. Lian, Z., Wang, L., Chen, Z., Wang, J., Yang, J., & Chang, Y. (2015). Plasmonic silver quantum dots coupled with hierarchical ZnO nanostructures for enhanced photocatalysis. *Scientific Reports*, 5, 10461. <https://doi.org/10.1038/srep10461>
17. Liu, Y., Zheng, Z., Liu, H., & Chen, G. (2019). Review on Ag-based plasmonic photocatalysts for organic pollutant degradation. *Journal of Materials Science & Technology*, 35(7), 1327–1341. <https://doi.org/10.1016/j.jmst.2019.03.024>
18. Luo, B., Liu, T., Zeng, M., & Yang, J. (2017). Ag/AgCl visible-light photocatalyst: A review. *Applied Catalysis B: Environmental*, 205, 523–548. <https://doi.org/10.1016/j.apcatb.2016.12.062>

19. Marimuthu, S., Antonisamy, A. J., Malayandi, S., Rajendran, K., Tsai, P.-C., Pugazhendhi, A., & Chang, S. W. (2020). Silver nanoparticles in dye effluent treatment: A review on synthesis, treatment methods, mechanisms, photocatalytic degradation, toxic effects and mitigation of toxicity. *Journal of Photochemistry and Photobiology B: Biology*, 205, 111823. <https://doi.org/10.1016/j.jphotobiol.2020.111823>
20. Mittal, A., Chisti, Y., & Banerjee, U. C. (2005). Synthesis of metallic nanoparticles using plant extracts and their properties. *Biotechnology Advances*, 23(3), 199–210. <https://doi.org/10.1016/j.biotechadv.2005.02.003>
21. Nazir, A., Tong, Z., Zhang, L., & Sun, H. (2023). A review on plasmonic-based heterojunction photocatalysts for environmental remediation. *Nanomaterials*, 13(6), 1062. <https://doi.org/10.3390/nano13061062>
22. Paul, K. K., Pradhan, B., Ghorai, U. K., & Pal, A. (2019). Evidence for plasmonic hot electron injection induced heterogeneous photocatalysis on semiconductor surface. *Applied Catalysis A: General*, 584, 117141. <https://doi.org/10.1016/j.apcata.2019.117141>
23. Ranjit, P., Palanivel, T., & Saravanakumar, A. (2022). A review on plasmonic metal-based photocatalytic systems for environmental applications. *Chemosphere*, 291, 132924. <https://doi.org/10.1016/j.chemosphere.2021.132924>
24. Saratale, R. G., Saratale, G. D., Kim, D. S., & Ghodake, G. S. (2018). Green synthesis of silver nanoparticles and their application in photocatalytic degradation of methyl orange. *Journal of Photochemistry and Photobiology A: Chemistry*, 361, 156–162. <https://doi.org/10.1016/j.jphotochem.2018.05.020>
25. Sepideh, H., Zarrabi, M., & Khataee, A. (2020). Synthesis and application of Ag-decorated photocatalysts for enhanced degradation of organic pollutants: A review. *Separation and Purification Technology*, 240, 116616. <https://doi.org/10.1016/j.seppur.2020.116616>
26. Shi, W., Lv, X., Li, X., Liu, Y., & Hou, Y. (2021). Recent advances in plasmonic photocatalysis with noble metal nanoparticles. *Chemical Society Reviews*, 50(19), 10839–10874. <https://doi.org/10.1039/D1CS00192F>
27. Xu, L., Zhang, L., Wang, Y., & Chen, X. (2025). Enhancing visible-light photocatalytic activity of AgCl by CeO₂ modification. *Nanomaterials*, 15(7), 537. <https://doi.org/10.3390/nano15070537>
28. Xu, Y., Chen, J., Feng, S., & Li, C. (2018). Silver-based visible-light plasmonic photocatalysts for organic degradation. *Chemosphere*, 205, 660–674. <https://doi.org/10.1016/j.chemosphere.2018.04.103>
29. Yang, H., Lu, Y., & Zhang, W. (2020). Plasmon-enhanced photocatalysis by Ag nanoparticles: Mechanism and applications. *Journal of Photochemistry and Photobiology C: Photochemistry Reviews*, 44, 100378. <https://doi.org/10.1016/j.jphotochemrev.2020.100378>
30. Zhou, L., Wang, J., Liu, P., & Linic, S. (2024). Plasmon-induced hot electrons in nanostructured materials. *Chemical Reviews*, 124(20), 10853–10928. <https://doi.org/10.1021/acs.chemrev.4c00165>